Journal of Advanced Research 34 (2021) 13–27

Contents lists available at ScienceDirect

Journal of Advanced Research

journal homepage: www.elsevier.com/locate/jare

Sustainable synthesis of rose flower-like magnetic biochar from tea waste for environmental applications

Kamyar Shirvanimoghaddam [a,*], Bożena Czech [b], Katarzyna Tyszczuk-Rotko [c], Magdalena Kończak [d], Seyed Mousa Fakhrhoseini [a], Ram Yadav [a], Minoo Naebe [a,**]

[a] Carbon Nexus, Institute for Frontier Materials, Deakin University, Geelong, Victoria 3216, Australia
[b] Department of Radiochemistry and Environmental Chemistry, Institute of Chemical Sciences, Faculty of Chemistry, Maria Curie-Skłodowska University, 3 Maria Curie-Skłodowska Sq., 20-031 Lublin, Poland
[c] Department of Analytical Chemistry, Institute of Chemical Sciences, Faculty of Chemistry, Maria Curie-Skłodowska University, 3 Maria Curie-Skłodowska Sq., 20-031 Lublin, Poland
[d] Institute of Earth and Environmental Sciences, Faculty of Earth Sciences and Spatial Management, Maria Curie-Skłodowska University, 2cd Kraśnicka Ave, 20-718 Lublin, Poland

GRAPHICAL ABSTRACT

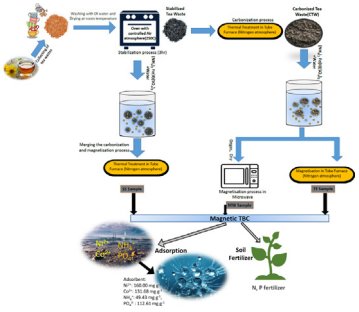

ARTICLE INFO

Article history:
Received 13 March 2021
Revised 7 July 2021
Accepted 3 August 2021
Available online 5 August 2021

Keywords:
Magnetic biochar
Microwave
Heavy metal removal
Nutrients removal
Fertilizer

ABSTRACT

Introduction: Biochar utilization for adsorption seems to be the most cost-effective, easy/fast approach for pollutants removal from water and wastewater. Due to the high adsorption properties, magnetic biochar proved to be efficient in the sorption of heavy metals and nutrients. Although there are several studies on development of magnetic biochars, there is a lack of research on development of high-performance magnetic biochar from food waste for removal applications.
Objectives: This study aimed at preparing new classes of magnetic biochar derived from tea waste (TBC) for removal of heavy metals (Ni^{2+}, Co^{2+}), and nutrients (NH_4^+ and PO_4^{3-}) from water and effective fertilizer (source of NH_4^+ and PO_4^{3-}).
Methods: Standard carbonization process and ultrafast microwave have been used for fabrication of TBCs. The removal of nickel, cobalt as the representatives of heavy metals, and over-enriched nutrients (NH_4^+ and PO_4^{3-}) from water were tested and the removal kinetics, mechanism, and the effect of pH, dissolved organic matter and ionic strength were studied. Simultaneously, possible fertilizing effect of TBC for controlled release of nutrients (NH_4^+ and PO_4^{3-}) in soil was investigated.
Results: Up to 147.84 mg g^{-1} of Ni^{2+} and 160.00 mg g^{-1} of Co^{2+} were adsorbed onto tested biochars. The process of co-adsorption was also efficient (at least 131.68 mg g^{-1} of Co^{2+} and 160.00 mg g^{-1} of Ni^{2+}). The highest adsorbed amount of NH_4^+ was 49.43 mg g^{-1}, and the highest amount of PO_4^{3-} was 112.61 mg g^{-1}.

Peer review under responsibility of Cairo University.
* Corresponding author.
** Corresponding author.
E-mail addresses: kamyar.shirvanimoghaddam@deakin.edu.au (K. Shirvanimoghaddam), Minoo.naebe@deakin.edu.au (M. Naebe).

https://doi.org/10.1016/j.jare.2021.08.001

The increase of the solution ionic strength and the presence of natural organic matter affected both the amount of adsorbed Ni^{2+}+Co^{2+} and the reaction mechanism.
Conclusions: The results revealed that magnetic nanoparticle impregnated onto tea biochar, can be a very promising alternative for wastewater treatment especially considering removal of heavy metals and nutrients and slow-release fertilizer to improve the composition of soil elements.

Introduction

The removal of pollutants from water using waste derived adsorbents has received significant attention lately [1–4]. One of the important adsorbents obtained from biomaterials is biochar. Biochar is derived from thermal decomposition of plant biomass in partial or total absence of oxygen [5–7]. Chemically, it is a char black carbon that comprises a large fraction of organic matter [1]. Biochars are widely studied due to their low cost and versatile applications [8,9] in agriculture such as improved soil fertility, water retention or crop yield [2,5,10], environmental protection and CO_2 capture [11], adsorption of organic [12], inorganic contaminants [12] and over-enriched nutrients (N and P) in aquatic environment) [13], as well as material studies [14].

The source for biochar can be agricultural, food, industrial, municipal and even hospital wastes [15–21]. Carbon rich feedstock such as bamboo, peanut shell, orange peel, pinewood, sludge, soybean Stover, switch grass, palm bark, corn straw and rice straw could be the idea precursors for development of biochar for different applications [8,9,13,22,23]. Increased production and consumption of food is connected with the production of food wastes that leads to many social and environmental challenges, however it can be considered as an inexpensive source of valuable components [24–28] including substrates and feedstock for biochar production.

Most biochar studies are focused on amendment, enhancement of crop yield and carbon storage [2]. In the last decade, the global attention for use of biochar for wastewater treatment has significantly increased. The difficulty in separating the powdered biochar from the environmental medium may lead to secondary pollution and hinder the large-scale application of biochar as an adsorbent [18]. The direct application of biochar in adsorption studies is associated with time and energy consuming recovery of the adsorbent. In this study, in order to facilitate the adsorption, process the magnetic biochar which is easy to be removed after the process was developed.

Microwave assisted pyrolysis (MWAP) is an alternative heating approach to convert organic waste materials into value-added products, such as biochar (BC) that can be used widely for environmental applications. The MWAP is a sustainable, cost-effective and environmentally friendly route in development of high-performance biochar [29,30]. Microwave (MW) valorization of biomass to biofuels represents an economically viable and harmless approach by virtue of high availability of raw materials, and thermochemical process with positive energy ratio [31].

Magnetization of biochar [18,22,28,29] can be obtained by various methods including i) impregnation-pyrolysis, ii) co-precipitation, iii) reductive co-deposition or iv) hydrothermal carbonization. The literature data on magnetization effect on biochar adsorption properties are indicating that different response can be noted both increased [18] or reduced [22,32] adsorption capacity. The application of Fe during biochar production [33] have an impact on biochar properties such as the adsorption ability and selectivity resulted from the surface modification and creation of ‘‘engineered biochar”.

Heavy metals are widely recognized as pollutants [34,35]. The toxicity of nickel (Ni) and cobalt (Co) is well known [34,36]. Their concentrations must be monitored in environmental matrices. The concentrations in drinking water should not exceed: 0.005 mg L^{-1} for cobalt [37] and 0.1 mg L^{-1} of Ni [38]. Nickel sources include incineration, batteries and industrial and domestic wastewater e.g. production of alloys or food processing, respectively [38]. In the environment, the main accumulation tank for Co and Ni is soil. The maximum permissible level of Co and Ni in agricultural soils is as follows: 39 and 420 mg/kg dry mass (d.m.) according to US EPA, and 20–40 and 300–400 mg/kg d.m. according to EU Commission [39]. Some trace metals tend to accumulate in the crops or vegetables. The literature data [40] indicate that Ni revealed higher tendency for accumulation in radish leaves than other metals such as Cr or Co. The concentration of heavy metals is found to be higher in the edible parts of plant (leaves and roots). Simultaneously, the enrichment of soil in Ni than Co when irrigated by the treated wastewater was found. Due to the bioavailability and toxicity of Co^{2+} and Ni^{2+} there is a need to develop new methods for their removal from water.

On the other hand, the presence of some nutrients in water or wastewater such as nitrogen (N, in the form of NH_4^+) or phosphorus (P, in the form of PO_4^{3-}) is responsible for the increased problem of eutrophication [41]. Apart from (un)treated wastewater, N and P source can be lost from soil, enriched when chemical fertilizers were additionally used [41]. The high level N-NH_4^+ is toxic to plants, bacteria and aquatic animals [41], whereas P is a major nutrient in soil possessing however lowest mobility and though phytoavailability [42].

Adsorption seems to be the most cost effective, easy and fast method for pollutants removal [6,7,16,43]. Due to the high adsorption properties, magnetic biochar can be used for sorption of both heavy metals and nutrients from aqueous solution. Although there are several studies on heavy metal adsorption onto magnetic biochars or biochars obtained from Hot Drinks Wastes [44], to the best of our knowledge this is the first report on use of easily separable [18] rose flower-like magnetic tea waste based biochar (TBC) for Ni^{2+}, Co^{2+}, NH_4^+ and PO_4^{3-} adsorption. The effect of magnetization type i) two step vs. one step carbonization, ii) microwave assisted carbonization, were tested. Additionally, the potential use of TBC as fertilizer for controlled release of nutrients in soil was estimated.

Experimental

Materials and methods

The household tea waste was used as the biochar precursor. The tea waste was washed and dried at room temperature prior to heat treatment in air at 250 °C (3hr). Three different approaches were used for magnetization process. For synthesis of the Tube furnace (TF) samples, heat treated tea wastes are firstly carbonized in argon atmosphere and then carbonized tea wastes (CTW) are subjected to the magnetization process in tube furnace. For making a microwave sample (MW), heat treated tea waste was first carbonized in tube furnace and then magnetization was performed in a microwave for 10 s using ammonium iron(II) sulphate. The last set of samples was single stage samples (SS) where the process of the carbonization of the stabilized tea waste and magnetization

were combined and performed in a tube furnace. The details of the processes are presented in Fig. 1.

For magnetization process, ammonium iron(II) sulphate (supplied by Chem-supply, X) was used. Using the thermal process, ammonium iron(II) sulphate which contains Fe(II) species is decomposed at 230 °C, and Fe(III) species appears according to the following reaction [29,30]:

$$2(NH_4)_2Fe(SO_4)_2 \rightleftarrows (NH_4)_2Fe_2(SO_4)_3 + (NH_4)_2SO_4 \quad (1)$$

As the presence of both iron species is required to form magnetite nanoparticles (MNPs), application of this unique double salt simplifies the complex Fe_3O_4 MNPs preparation method·H_2O molecules are formed by dehydration of the compounds and at 450 °C $Fe_2(SO_4)_3$ and $FeSO_4$ are formed by the decomposition of the salt [45,46]. During the heat treatment process, the conversion of Fe-based structure to Fe_2O_3 occurred at ~640 °C [47,48] and Fe_3O_4 nanoparticles are formed by thermal conversion of Fe_2O_3 in inert atmosphere(Nitrogen) [49]. Formation of Fe_3O_4 magnetic nanoparticles on the surface of tea waste or carbonized tea waste were carried out by immersing the CTW in an aqueous solution of ammonium iron(II) sulphate. To remove remained air in samples and accelerate the ion transfer into structure, samples are subjected to degassing process in vacuum chamber for 30 min. Surface decoration of CTW with MNPs was carried out by a very intense heating sequence in a microwave oven (LG 1100Watt) for 2 cycles of 10 s in MW samples. In case of TF and SS samples, the process of magnetization was performed in a tube furnace (10 °C min^{-1}, dwelling time (1hr) at 800 °C). The samples are tested for BET surface area using low temperature N_2 adsorption and BET method in Autosorb Quantachrome and structural imaging were performed using a Zeiss Supra TM 55VP SEM.

Sorption experiment

Sorption was monitored in the batch experiments in 40-mL Teflon centrifuge tubes. Three biochars (50 mg) and an initial 10 mg L^{-1} concentration of Ni^{2+} and/or Co^{2+} and 50 mg L^{-1} of NH_4^+ or/and PO_4^{3-} were used in biocide background solution (0.01 mol L^{-1} $CaCl_2$ and 3.08 mmol L^{-1} NaN_3 in deionized distilled water). Samples were shaken in the dark (rotary shaker 200 rpm) for seven days at ambient temperature (23 ± 1 °C).

The adsorption experiments over the pH range 5–9 for NH_4^+ and 5.8–9.15 for PO_4^{3-} and 2–6.54 for Co^{2+} and Ni^{2+} were performed to find an optimal pH. Solution pH values were adjusted with 0.1 M HCl and/or 0.1 M NaOH.

Sorption kinetics was monitored in the batch experiments in 40-mL Teflon centrifuge tubes. Biochars (50 mg) and an initial 20 μg L^{-1} concentration of Ni^{2+}, Co^{2+} and 50 mg L^{-1} of NH_4^+ and PO_4^{3-} were prepared in biocide background solution at pH_{Co} = 6.4, pH_{Ni} = 6.4, pH_{Co+Ni} = 6.4, pH_{NH4+} = 6.60, pH_{PO43-} = 7.88, $pH_{NH4++PO43-}$ = 7.47 being the most suitable according to the obtained results of the studies.

Samples were shaken in the dark (rotary shaker 200 rpm) at ambient temperature (23 ± 1 °C). At selected time intervals (2, 8,

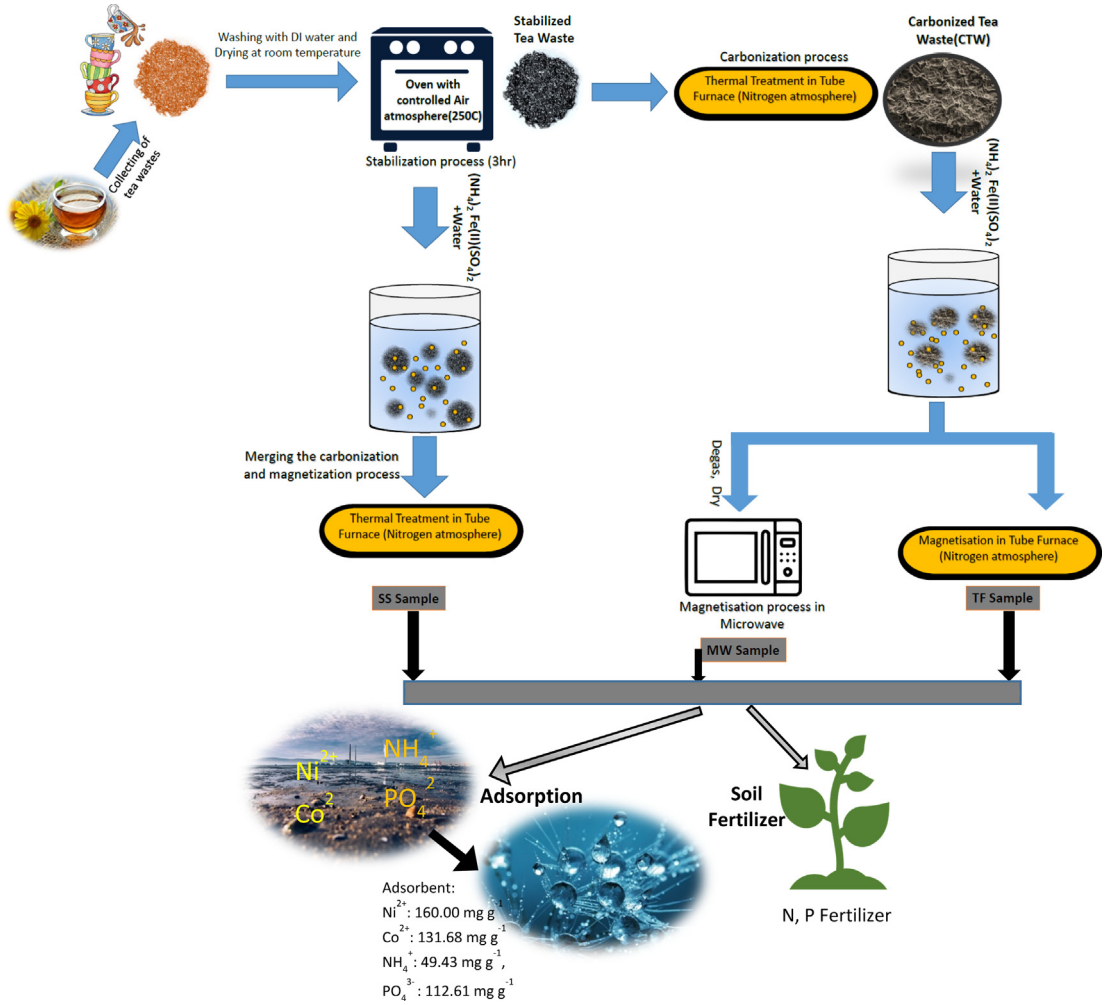

Fig. 1. Schematic diagram of developing of magnetic tea waste biochar.

24, 48, 72 and 168 h) tubes were centrifuged (1000g for 20 min) and the mass of adsorbed ions was determined. The adsorbed mass was calculated based on the decrease of the solute concentration in the aqueous phase. There was no measurable change in concentrations in the control vials.

For the determination of adsorption isotherms, a batch equilibration technique at 23 ± 1 °C in the dark was employed using 50 mg of TBC in the background solution and 10–100 mg L^{-1} of tested solutions. The tubes were shaken (200 rpm) and after seven days (adsorption time necessary to obtain equilibrium obtained in preliminary studies), the tubes were centrifuged and the concentration of adsorbates in solution phase was determined by appropriate methods. Each concentration point, including blanks, was run in duplicate.

The effect of ionic strength was assessed using NaCl solutions in the range of 0–100 mM Na^+. Simultaneously the effect of dissolved organic matter was estimated using tannic acid solutions 0–100 mg L^{-1}. In the end, the test with agricultural soil was performed using 1 g of tops soil samples (0–20 cm) from Lublin area (Poland), previously dried at 40 °C and sieved (2 mm). To soil a TBC (50 mg) and 40 mL of NH_4^+ + PO_4^{3-} solution (50 mg L^{-1} each) were added The samples were covered in aluminum foil and shaken (200 rpm) for 6 days. The amount of NH_4^+ + PO_4^{3-} was estimated in supernatant after centrifugation.

Ions and data analysis

The voltammetric measurements of Co^{2+} and Ni^{2+} were performed using μAUTOLAB analyzer (Eco Chemie, The Netherlands) controlled by GPES 4.9 software in a 10 mL electrochemical cell with a lead film glassy carbon electrode (PbF/GCE) as a working electrode, Pt wire and Ag/AgCl, KCl (3 mol L^{-1}) as auxiliary and reference electrodes, respectively [50].

NH_4^+ and PO_4^{3-} ions were analyzed using the MIC 3 ion chromatographer by Metrohm. A SUPP 5 250 analytical column (eluents: sodium bicarbonate/sodium carbonate concentrate - Sigma Aldrich, flow rate 0.7 mL min^{-1}) and a Metrosep C4 150 analytical column (eluent: Nitric acid/Dipicolinic acid concentrate - Sigma Aldrich, flow rate 0.9 mL min^{-1}) were applied for anions and cations analysis, respectively. Conductometric detection for both cation and anion analysis was conducted [51,52].

For the description of Co^{2+}, Ni^{2+}, NH_4^+ and PO_4^{3-} adsorption four kinetic models: pseudo first (PFO), pseudo-second order (PSO), Elovich and Intraparticle diffusion model (IPD) were applied. Langmuir (L), Freundlich (F), Temkin (T) and Dubinin-Radushkevich (DR) models were used for the testing of the adsorption isotherms. Detailed information about the models, kinetic curves, and isotherm fitting are presented in the Supporting Information (Table S1).

Table 1
Surface properties of tea biochar.

Sample	Surface Area(m^2/g)	Pore Volume (cc/g)	Pore Diameter (nm)
MW	41.259	0.077	4.175
SS	184.460	0.084	3.933
TF	111.215	0.201	1.5656

Results and discussion

Structural and surface properties

The details of the BET results and surface properties of the TBC are included in Table 1. As clearly seen, sample SS showed the highest surface area, while MW sample exhibited the lowest surface area. Except the MW sample, TF and SS samples showed acceptable surface area in the category of carbonized biochar for removal applications. SS sample showed higher surface area than activated tea waste in H_2SO_4 [53]. In case of pore diameter, sample TF showed a very small pores size (1.5 nm) compared to 3.93 and 4.17 nm for SS and MW samples, respectively. This is in agreement with the pore volume of the samples that showed the highest for TF sample compared to SS and MW samples. It is evident that a

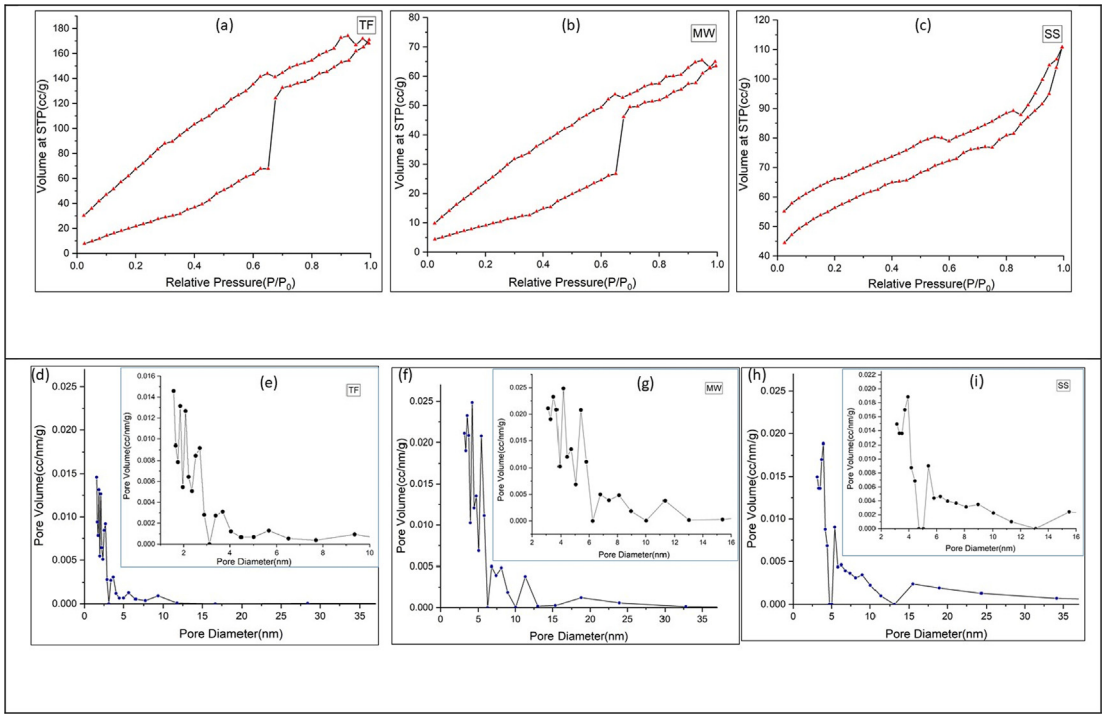

Fig. 2. Isothermal absorption/desorption patterns (a, b, c) and Pore size distribution (d-i) of different zea biochar.

large number of small pores and a small number of large pores are seen for sample TF. In case of MW and SS samples, they showed a broad range of pore size ranging from 4 nm to more than 10 nm (see Fig. 2).

SEM micrographs of the CTW and TF sample are shown in Fig. 3. The rose flower like pattern of CTW with a central void is observed for all samples. After the magnetization, the nanoparticles that absorbed onto the surface, have been converted into the Fe_3O_4

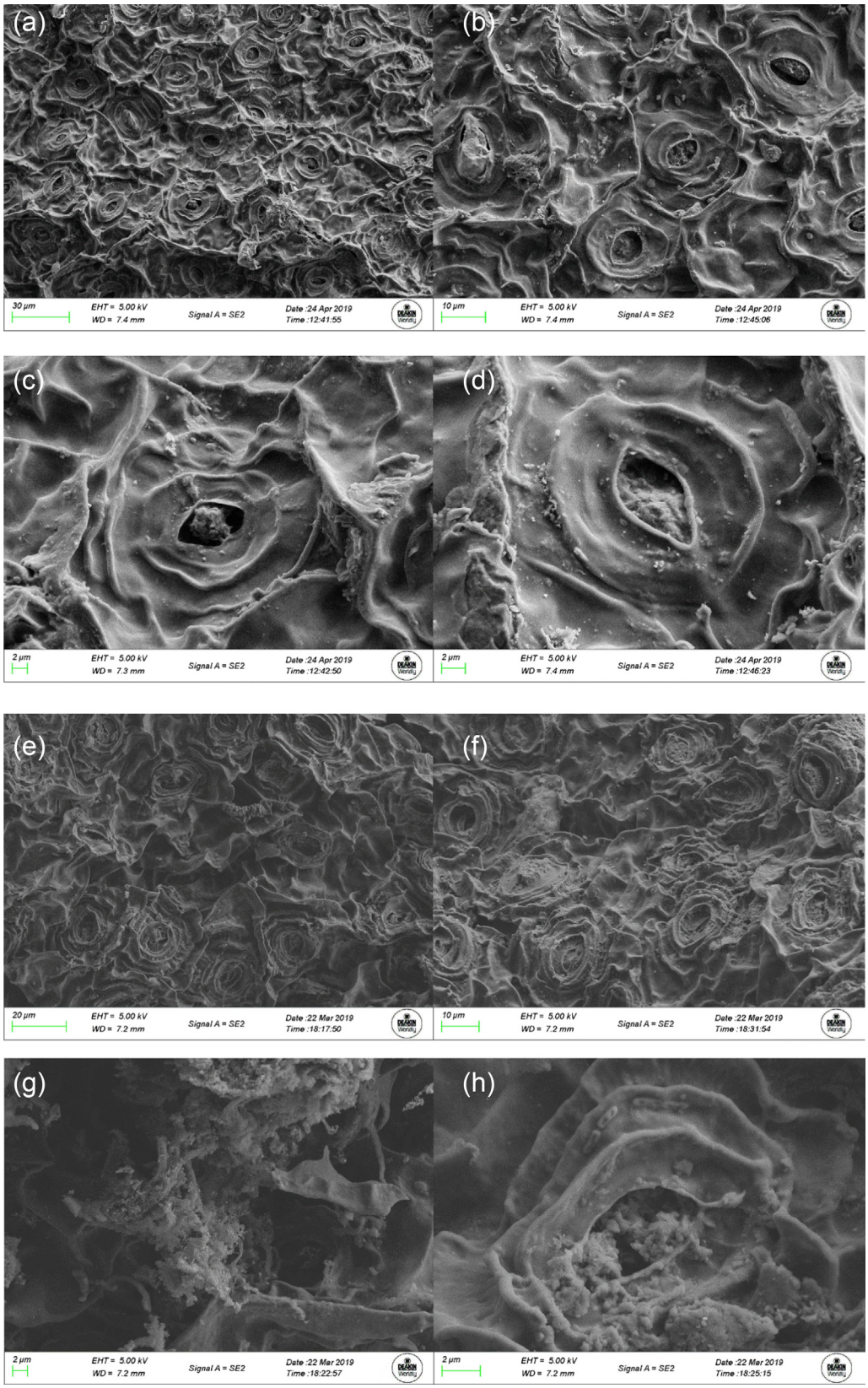

Fig. 3. Structural Imaging of the CTW (a–d) and TF sample (e–h) showing the magnetic nanoparticles decorated on the surface.

magnetic nanoparticles and distributed on the surface homogenously. As can be seen some areas seems to be more attractive for adhesion of nanoparticles due to lower surface energy such as the void in the center of the rose flower (see Fig. 3H). It is observed that there are numerous macroscopic pores and nanopores in particular in the void area of the rose flower which may be due to the release of gases from the core towards the outer surface of precursor and also carbonization and removal of non-carbon atoms in forms of water and oxides of nitrogen and carbon from the material [53]. It can be concluded that carbonization and magnetization process resulted in the development of porous structure in tea waste based biochar.

FT-IR spectra presented in Fig. 4 indicate that the surface of TBC was enriched in surface functionalities. TW before (Fig. 4A), both raw and stabilized and after carbonization were possessing several surface functional groups. Bands at ~2900 and 2840 and cm^{-1} were confirming the presence of CH_3 groups both in aromatic rings and alkanes (C-H stretching) resulting from the presence of lignin and holocellulose [33].

The characteristic peaks at 3400–3300 cm^{-1} 3188 cm^{-1}, 2842 cm^{-1}, 1651 cm^{-1}, 1518 cm^{-1}, 1047 cm^{-1} and 852 cm^{-1} were responsible for stretching of N—H, =C—H sp^2, C—H for methyl, C=O, aromatic C=C, alcoholic C—O and C—O—C and out-of-plan aromatic C—H bending vibrations, respectively [54].

Fig. 4C and D represents results of Raman spectroscopy analysis on tea wastes biochars, before and after magnetization. Since the stabilized and carbonized Tea wastes will be subjected to a harsh MNPs growth reaction, study of graphitic structure of the CMT substrate provide the idea of the how the microwave assisted MNPs formation reaction is working. As a rule, the higher graphite content of carbonaceous materials enhances the joule heating mechanism and results in the higher microwave absorption at the same reaction condition [17,55–58]. Based on the presented Raman spectra in Fig. 3A, the MNP characteristic peak is observed when the laser spotted at an accumulation of nanoparticles. After microwave assisted magnetization, the ID/IG ratio and a substantial growth in the ratio was observed in comparison to STW and CTW samples. The higher disordered ratio in magnetized samples

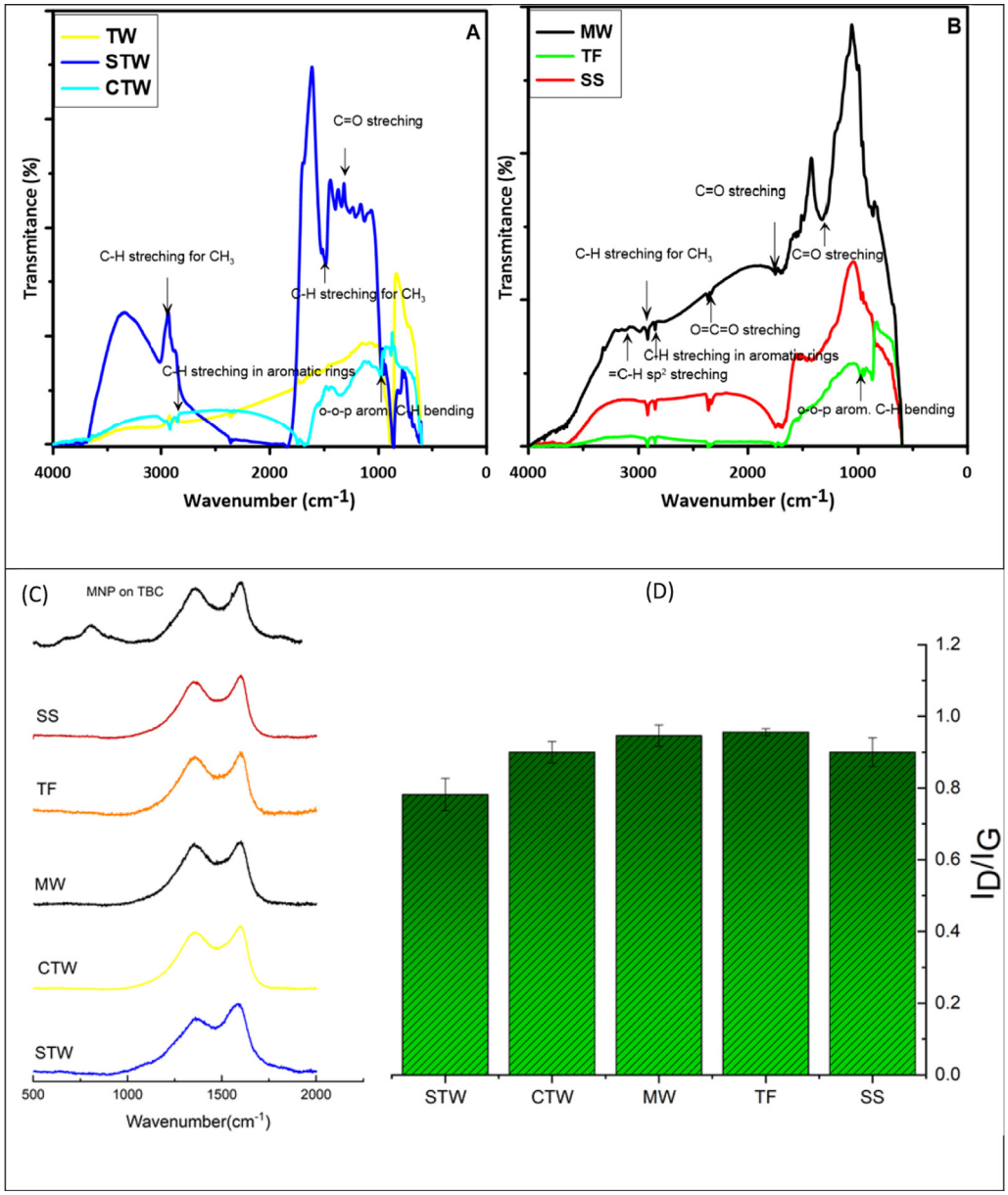

Fig. 4. FT-IR spectra of (A) TW, STW and CTW and (B) TBCs. Raman spectroscopy on surface of MNPs decorated Magnetized Tea waste biochars and quantified ID/IG ratios, (C) Raman spectra on all samples and for a nanoparticle rich location on TBC (the top spectrum), (D) the average ID/IG ratio of samples before and after magnetization.

is due to the higher microwave absorption of TBCs and related to the size of graphite crystallites.

Adsorption studies

In order to evaluate the releases of readily soluble ions from TBC, they were extracted by cold DI water. Results of the readily soluble ions are presented in Table 2.

It can be seen that the obtained biochar differ in content of soluble ions. Highest initial content of PO_4^{3-} was noted in SS sample, and NH_4^+ in MW sample. The highest pH was obtained for TF and SS samples. Increased pH may imply the presence of inorganic alkaline components in the biochars [59].

pH effect

In the first stage of the adsorption study the most preferential adsorption conditions for all tested ions and TBC were selected (Fig. 5). pH have an effect on the adsorbent's surface charge, the degree of ionization and the speciation of adsorbates [40]. The obtained data clearly indicate that the optimum pH conditions for adsorption onto MW TBC are: Ni – 6, Co – 2 (however at pH = 6, 81% of C_s in strong acid conditions were noted), NH_4^+ – 7.14, PO_4^{3-} – 7.2), SS: Ni – 4, Co – above 5.6, NH_4^+ – 6–9, PO_4^{3-} – 9; TF: Ni – 6, Co – 5, NH_4^+ – 9, PO_4^{3-} – 7.2.

At low pH, the competition between NH_4^+ and H^+ was responsible for lower adsorption, similarly to the competitive effect of NH_4^+ and OH^- reaction in the solution at higher pH values [60] or created at high pH $NH_3{\cdot}H_2O$, is less favorable for ion exchange [41].

Generally, at higher pH values, the precipitation of metal hydroxides is observed. For Ni the pH of precipitation is 10–11, whereas for Co it starts at 6.9 [61], though the tests were performed up to pH = 7 for Ni and Co adsorption. The observed increase of C_s of Ni or Co with increased pH was connected with the fact that at lower pH values, the concentration of H^+ was very high competing with metal cations and the ion exchange site onto TBC hindering adsorption. At higher pH values, lower concentration of H^+ was noted and higher adsorption of Ni or Co, occurred via the ion exchange [62]. Under acidic conditions in the environment the mobility of Ni is increased implying the enhanced availability. As the noted effect was not strictly linear, the adsorption studies were further conducted without pH adjustments based on initial concentration of applied salt.

Adsorption of NH_4^+ or PO_4^{3-} affected pH noted at the end of the process. Although TF sample possessed highest pH, adsorption of NH_4^+ lowered this value much more than in case of SS sample. During NH_4^+ adsorption, SS surface properties were changed in the highest extend. Acidic surface of MW during PO_4^{3-} adsorption possessed the lowest pH after adsorption. Typically, the surface of biochars can be negatively charged and application of magnetization affected surface charge [18] and the observed effect was strictly connected with magnetization process type. Microwave magnetization was connected with creation of the most acidic surface among tested TBC, that was confirmed by FT-IR studies (=CO, —COO surface functional groups).

Generally, at pH 2–7 $H_2PO_4^-$ is dominating whereas HPO_4^{2-} is most abundant when pH is 7–12, and at pH 4–10 phosphate existed in both forms of HPO_4^{2-} and $H_2PO_4^-$ in solution affecting surface electrostatic interactions between phosphate ions and TBC negatively charged surface resulting in low PO_4^{3-} adsorption in comparison to other adsorbates. Surface of TF and SS during PO_4^{3-} adsorption was not prone to pH changes. However, at very high pH values (>10) increased electrostatic repulsions between the negative surface of TBC and the increasingly multivalent P oxyanions (pKa_2 = 7.21, pKa_3 = 12.67) can be observed. TBC can be applied for the removal of nutrients from water, especially that

Table 2
Composition of water solution of TBC after 3 days contact with water (n = 3).

Sample	Anions (mg·L^{-1})						Cations (mg L^{-1})					pH
	Cl^-	NO_2^-	Br^-	NO_3^-	PO_4^{3-}	SO_4^{2-}	Na^+	NH_4^+	K^+	Ca^{2+}	Mg^{2+}	
MW	1.85 ± 0.1	0.44 ± 0.02	NA	2.11 ± 0.09	0.68 ± 0.03	34.0 ± 1.5	0.85 ± 0.03	1.27 ± 0.06	3.25 ± 0.15	5.536 ± 0.2	0.83 ± 0.03	4.58
SS	1.21 ± 0.05	0.01 ± 0.001	0.087 ± 0.004	1.899 ± 0.08	3.445 ± 0.15	4.167 ± 0.18	0.315 ± 0.01	0.118 ± 0.01	1.898 ± 0.01	8.168 ± 0.35	0.47 ± 0.02	9.63
TF	0.614 ± 0.03	NA	0.099 ± 0.004	1.745 ± 0.07	1.333 ± 0.05	0.148 ± 0.01	0.362 ± 0.01	0.052 ± 0.002	1.871 ± 0.07	7.067 ± 0.3	0.542 ± 0.02	9.77

n - number of replicates.

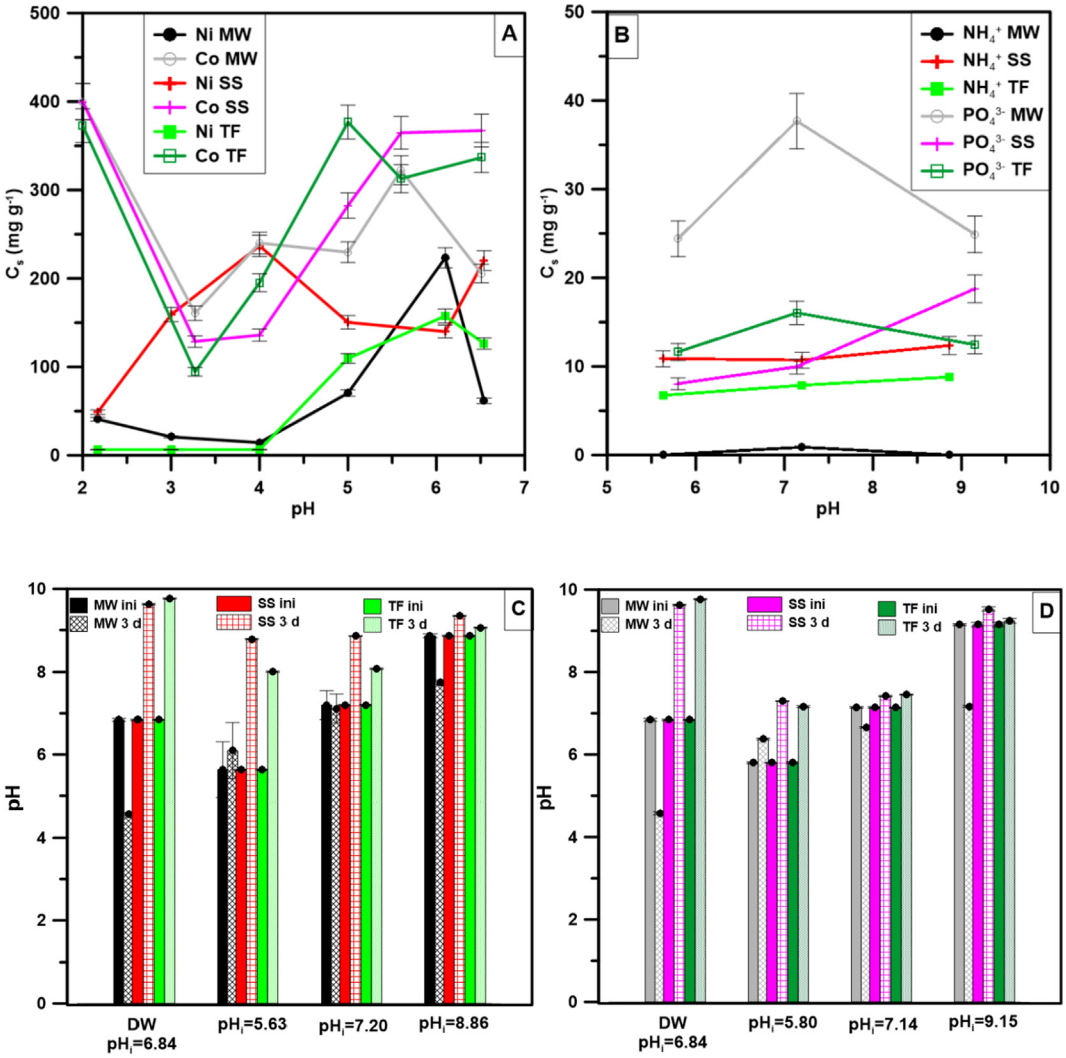

Fig. 5. Effect of pH on (A) Ni^{2+} and Co^{2+} adsorption, (B) NH_4^+ and PO_4^{3-} onto TBC, (C) changes of pH after sorption of NH_4^+ and (d) changes of pH after sorption of PO_4^{3-} from different solutions.

natural eutrophic waters are characterized by pH from 7 to 9 and P < 1 mg L^{-1} [42]. Similar effect was noted in the studies of Wan et al. [62] or Cai et al. [42].

Kinetics

In order to investigate the mechanism of adsorption and potential rate controlling steps such as mass transfer and chemical reaction process the kinetics of Ni^{2+}, Co^{2+}, Ni^{2+}+Co^{2+} and NH_4^+ +PO_4^{3-} adsorption was tested using four well known and widely tested kinetic models: pseudo-first order (PFO), pseudo-second order (PSO), Elovich and Intraparticle diffusion (IPD) that were described in Supplementary Information (Table S1).

The kinetic of Ni^{2+} and/or Co^{2+} adsorption onto TBC was presented in Fig. 6 and Table S2. It can be seen that the adsorption of Co^{2+} and Ni^{2+} was fast and more than 51% of Ni^{2+} and Co^{2+} from single solute system, and 56% and 50% from Ni^{2+}+Co^{2+} mixture, respectively, was adsorbed in first 8 h. However, adsorption of Co^{2+} was faster than Ni^{2+}. Generally, the amount of adsorbed Ni^{2+} after 7 days of sorption process was similar for all TBC and q_{eNi} was 144.84–147.84 mg g^{-1}, whereas q_{eCo} was 160.00 mg g^{-1}. In the mixture it can be observed that the presence of Ni^{2+} lowered Co^{2+} adsorption only onto SS TBC (from 145.76 to 131.68 mg g^{-1}). In case of the other TBC, the obtained q_e values were as high as 160 mg g^{-1}. This imply that SS surface is preferential to Ni^{2+} and Co^{2+} co-adsorption, maybe due to the highest surface area (184.460 m^2 g^{-1}) where there was enough place for adsorption of these two ions [61]. In the multi component solutions there is enough space for adsorption sites for both metals [63].

Co-adsorption of NH_4^+ and PO_4^{3-} was not favorable onto tested TBC in comparison to Ni^{2+} and/or Co^{2+} (Table 3). NH_4^+ adsorption was fast – in first 5 h at least 65% of maximum adsorption was noted. The adsorption of PO_4^{3-} onto SS and TF was lower than NH_4^+, after 5 h was 45% of PO_4^{3-} was adsorbed. The highest amount of NH_4^+ was adsorbed onto SS (49.43 mg g^{-1}), and the highest amount of PO_4^{3-} was noted onto MW (112.61 mg g^{-1}). These values were significantly higher than to those obtained in the studies of Wang et al. [13] (4.13 mg g^{-1} NH_4^+ and 19.75 mg $g^{-1}P$$O_4^{3-}$), Cai et al. [42] (2 mg g^{-1}P), Lu et al. (19.26454 mg g^{-1} min^{-1}) [60] or Wan et al. (5.21 mg g^{-1} for PO_4^{3-} [62]) but slightly lower than Xie et al. (64.90 mg g^{-1} NH_4^+-N [41]) or similar to Li et al. (121.25 mg g^{-1}P [64]).

Generally, the sorption studies indicated that over SS and TF TBC surface there were less adsorption sites for anions on the surface and PO_4^{3-} have to compete with NH_4^+ for the free adsorption sites. It was noted in literature that biochar with relatively high alkalinity (pH 7–12) was characterized by a low anion exchange capacity (<5 c_{mol} kg^{-1}) and very limited sorption capacity towards

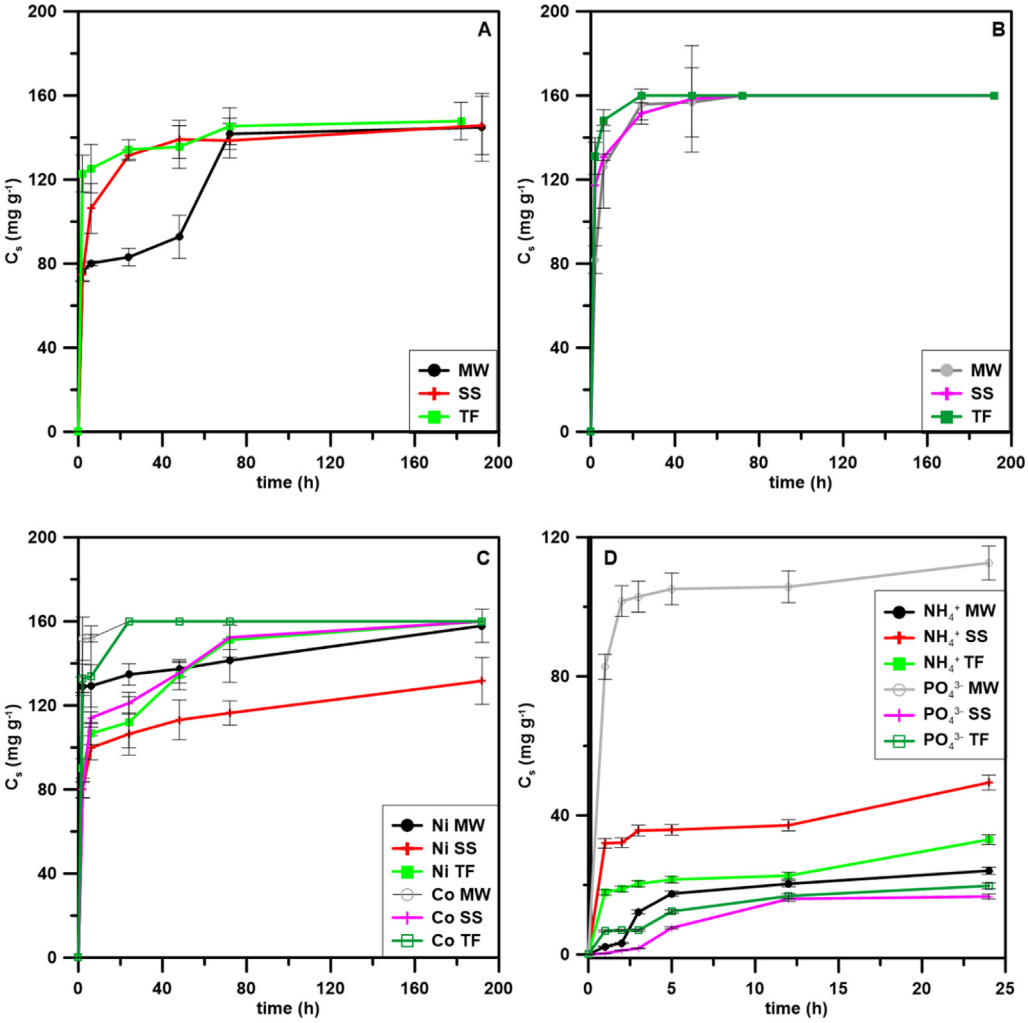

Fig. 6. Kinetics of (A) Ni^{2+}, (B) Co^{2+}, (C) Ni^{2+}+Co^{2+}, (D) NH_4^+ and PO_4^{3-} adsorption onto TBC.

the negatively charged anions, such as PO_4^{3-} [42]. The overall removal capacity for the different ions was as follows:

MW: Co^{2+}>Ni^{2+}> PO_4^{3-} > NH_4^+
SS: Co^{2+}>Ni^{2+}> NH_4^+ > PO_4^{3-}
TF: Co^{2+}>Ni^{2+}> NH_4^+ > PO_4^{3-}

Chemisorption was the rate limiting step during adsorption Ni^{2+} and Co^{2+} from single solute system and mixture solution. The R^2 values higher than 0.997 were confirming a great fitting of experimental data of Ni^{2+}, Co^{2+}, Ni^{2+}+Co^{2+} adsorption to the PSO model. Additionally, the calculated q_{2eq} in PSO were similar to the $q_{e\ exp}$. Interestingly, the process of NH_4^+ adsorption onto MW and PO_4^{3-} adsorption onto SS revealed a best fitting to Elovich model. Considering the Elovich model parameters, higher value of α than β indicated higher adsorption rate than desorption. PSO regime is the mostly applied for the description of adsorption of metals and nutrients onto biochars [13,41,42]. Elovich model was also describing the adsorption of tetracycline onto mesoporous tea waste derived biochar [65].

Considering the mechanism of diffusion, a good fitting of film diffusion can be observed only in case of PO_4^{3-} onto all TBC, NH_4^+ onto SS and TF samples, Ni^{2+} in Co^{2+} presence onto all TBC; however, film diffusion might not be the sole rate-limiting step. In the studies of Hokkanen et al. [61], although PSO regime revealed a good fitting, higher applicability for Ni^{2+} and PO_4^{3-} adsorption revealed PFO.

The positive correlation between k_2 noted for Co^{2+} adsorption and pore volume was noted ($p < 0.05$) confirming the role of pore filling mechanism and participation of pores in adsorption. However, negative correlation with pore diameter ($p < 0.001$) indicates that the pore with lower diameter were preferred for Co^{2+} adsorption onto TBC. In Ni^{2+} adsorption in Co^{2+} presence the key point is surface area of TBC ($p < 0.1$), however, again, lower surface area was preferred in Ni^{2+} adsorption. No correlation between k_2 during NH_4^+ or PO_4^{3-} adsorption and TBC properties was noted.

In IPD model two phases can be observed expressed as two linear regions in IPD curve. The first fast step was connected with the spread of ions on TBC surface. k_{id1} was higher usually than kid indicating that the process was fast whereas low k_{id2} values inform on slow process of ions adsorption [60]. Due to the fact that the intercept of linear form is not zero, then intraparticle diffusion is not a regnant mechanism and does not determine the mass transfer rate in the adsorption process [60]. If k_{id1} is higher than k_{id2} [66] the faster rate of film diffusion than intraparticle diffusion is considered. Interestingly, Ni^{2+}, Co^{2+} and NH_4^+ adsorption onto MW was governed by intraparticle diffusion than film diffusion. It was concluded that the adsorption kinetics might be controlled by both film diffusion and intra-particle diffusion simultaneously [66].

Isotherms

The adsorption isotherms were nonlinear indicating a clear dependence of the sorption capacity from the ions concentration. Four nonlinear isotherm models (Freundlich, *F*, Langmuir, *L*, Temkin *T*, and Dubinin-Radushkevich, *DR*) were tested to fit the experimental data. Application of *L, F, T* or *DR* models had the highest coefficient of determination (R^2) (Table S2).

R^2 values were as high as 0.94 indicating good fitting of experimental data to tested models; however, there were two fittings with lower R^2 value (0.85 and 0.74), that were describing PO_4^{3-} adsorption onto MW and TF. Langmuir model indicating monolayer surface coverage onto homogeneous surfaces [67] was describing the adsorption of Ni^{2+} onto MW, Co^{2+} in the presence of Ni onto MW, and NH_4^+ onto MW, SS and TF TBC (Table S2, Fig. 7). Q_L describes the monolayer coverage and represents the practical limiting adsorption capacity, whereas K_L (L mg^{-1}), Langmuir equilibrium constant, is related to the affinity of the binding sites (the bond energy) for the adsorption reaction between metal and material [61]. The larger the K_L, the stronger the bond between adsorbate and adsorbent [60]. In *L* model, the highest Q_L (maximum amount adsorbed) was noted for NH_4^+ adsorption onto MW (1633.28 mg g^{-1}) indicating the highest adsorption capacity of MW towards NH_4^+. Simultaneously, the adsorption capacity of SS sample towards NH_4^+ adsorption was the lowest. Q_L in PO_4^{3-} adsorption onto tested TBC was negatively correlated with pore volume ($p < 0.1$) indicating that wide pores were available firstly as adsorption sites. The data included in Table S2 show that the Langmuir isotherm was favorable ($0 < R_L < 1$). Langmuir model was also applied for the description of NH_4^+ adsorption onto La-modified biochar produced from oak sawdust (Q_L = 10.1 mg g^{-1}) [13], PO_4^{3-} adsorption onto protonated g-C_3N_4 and acid-activated montmorillonite composite [62], MgO decorated biochar [64] or organics removal over tea waste biochar [68–70].

More complicated mechanisms e.g. the surface heterogeneity or interactions between adsorbing species were noted in case of the other adsorbates and adsorbents [61]. The process of Co^{2+} adsorption form single solute system was ascribed to *F* model and multilayer adsorption. Good fitting of *F* model was also noted in case of Ni^{2+} adsorption onto SS, and Ni^{2+} in Co^{2+} presence onto SS. In the Freundlich model, sorption onto sites with different energy is assumed and the energy of sorption sites depends on the degree of surface coverage with adsorbate molecules and the interactions between adsorbed molecules. In *F* model the highest value of Q_F (the relative adsorption capacity) was noted for Co^{2+} adsorption onto SS sample (152.127 mg·g^{-1}). The value of *1/n* (parameter related to linearity) is above 1 indicating unfavorable adsorption and its chemical character [53].

Adsorption of Ni^{2+} onto TF, Ni^{2+} in Co^{2+} presence onto TF, Co^{2+} in Ni^{2+} presence onto SS and TF and PO_4^{3-} onto MW was fitted Temkin

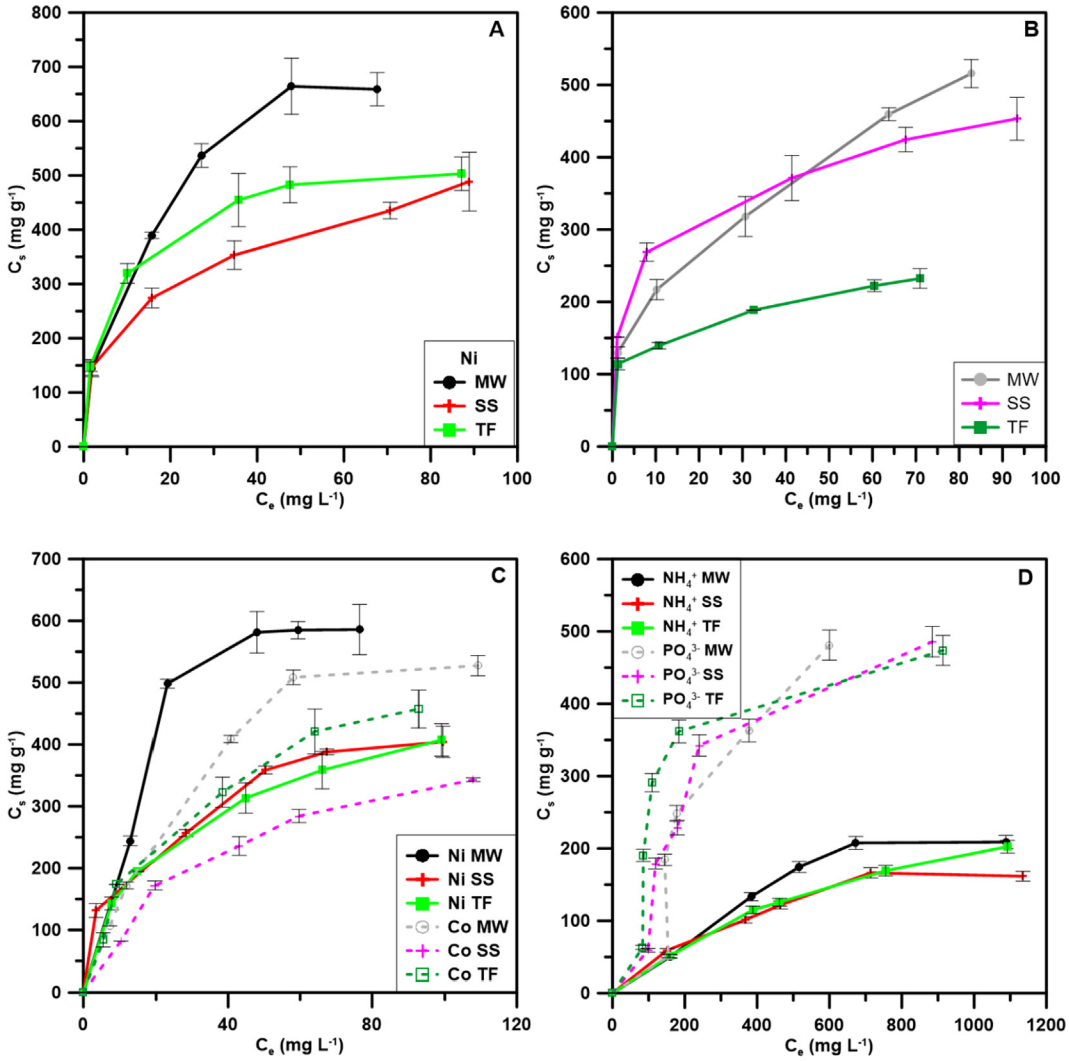

Fig. 7. Isotherms of (A) Ni^{2+}, (B) Co^{2+}, (C) Ni^{2+}+Co^{2+}, (D) NH_4^+ and PO_4^{3-} adsorption sorption onto TBC.

model. *T* model is considering heterogeneity of the surface. The highest Q_T was noted for Ni^{2+} adsorption onto TF sample – 3.350 mg g^{-1}. The other parameter, *B* - heat of adsorption, can be used to distinguish physical and chemical adsorption mechanism. The highest *B* value was noted for Ni^{2+} adsorption onto TF, 26.86 J mol^{-1}. The conversion of *B* values from J mol^{-1} to kcal mol^{-1} resulted in low values < 1 kcal mol^{-1} what indicates that physical sorption was dominant.

DR model can be used for the description of Ni^{2+} adsorption in Co^{2+} presence onto MW and PO_4^{3-} onto SS or TF. The highest Q_D value was noted in Ni^{2+} adsorption onto TF in the presence of Co^{2+} (624.05 mg g^{-1}). According to *DR* model the adsorption occurs onto heterogeneous surfaces of adsorbent [71] and is related to micropores volume filling as opposed to layer-by-layer adsorption on pore walls [72]. It can be clearly seen that the addition of co-solute in case of metals changed the mechanism of adsorption, for example onto MW, where Ni^{2+} was adsorbed by monolayer and after Co^{2+} addition the highest impact of pore filling was revealed. The highest Q_{DR} was noted for Ni^{2+} adsorption in Co^{2+} presence onto MW (624.05 mg g^{-1}). The obtained mean free energy (*E* greater than 8 kJ mol^{-1}) indicated a chemisorption process. Comparison of *E* values between metals and nutrients indicated that heavy mental ions revealed more affinity to ion-exchange process [41]. Similarly, Q_{DR} values were lower than Q_L what may indicate that not all micro/macrospores were occupied with solute [41].

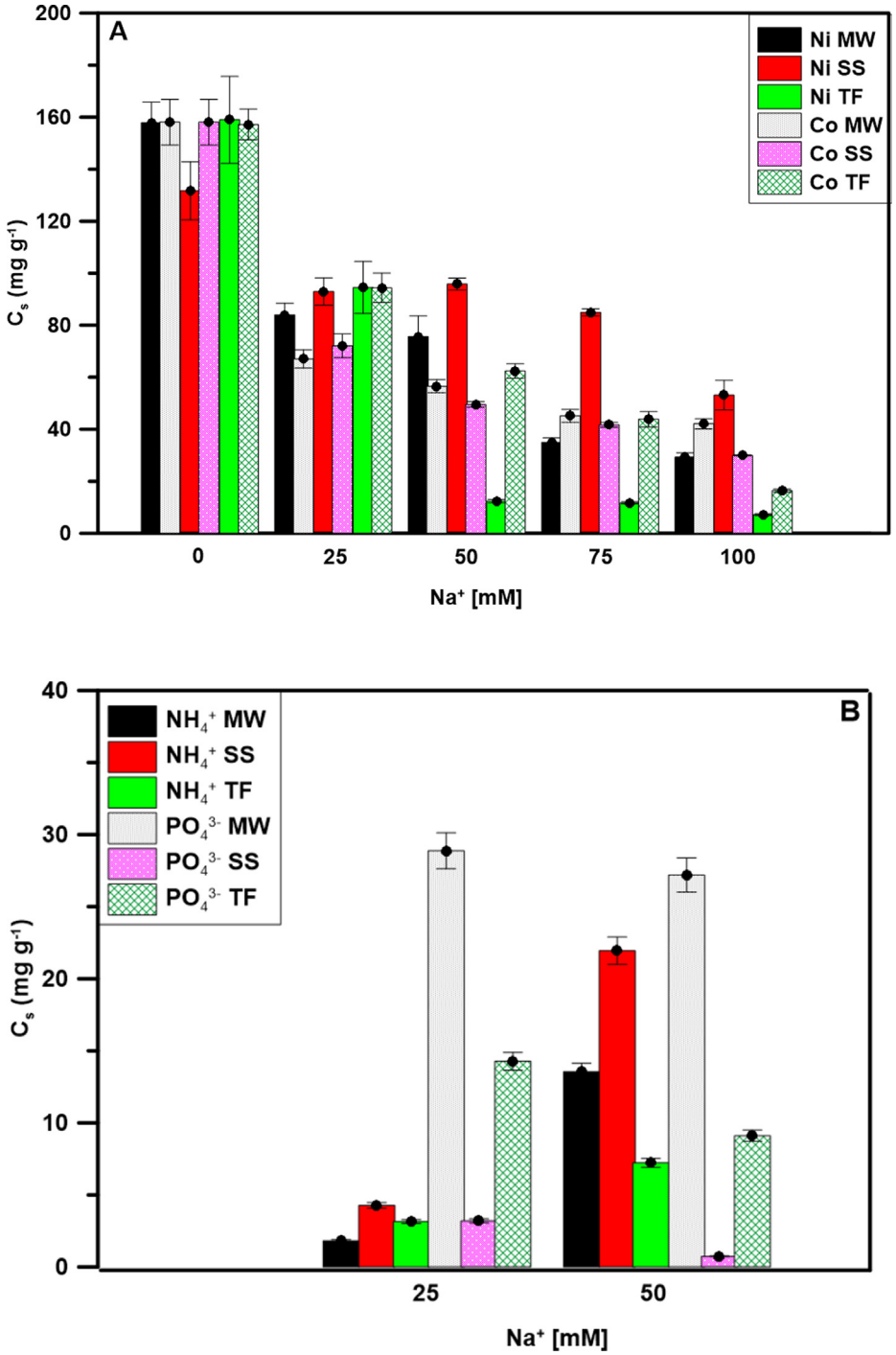

Fig. 8. Effect of IS on Ni^{2+}+Co^{2+} and NH_4^++PO_4^{3-}sorption onto TBC.

Several mechanism of adsorption of cationic heavy metals onto magnetic biochar were proposed: 1) electrostatic adsorption; 2) ion (ligand) exchange; 3) surface or inner-sphere complexation; 4) π-π interaction; 5) internal spherical complexation; 6) hydrogen bonding; 7) co-deposition [18]. All these mechanism can contribute to adsorption onto TBC [69]. However, adsorption process is affected both by the character of adsorbent (characteristics of the binding sites (e.g. functional groups, structure, surface properties, etc.), and the properties of the adsorbate (e.g. concentration, size, charge, molecular structure, pH, ionic strength, co-solvents etc.) [61]. The main surface groups onto TBC that participate in adsorption are graphite or aromatic carbon (C–C, C–H), alkoxy (C–O), carbonyl (C = O) and carboxyl (COOH) functional groups [18]. PO_4^{3-} adsorption was observed via electrostatic interaction H-bonds, whereas metal cation were adsorbed with the participation of complexation and electrostatic interaction [8].

Ionic strength effect

It can be clearly seen from the Fig. 8 that the increase of the solution ionic strength (IS) affected Ni^{2+} and Co^{2+} adsorption onto tested TBC: the greatest effect was noted in case of TF. In case of NH_4^+ + PO_4^{3-} interestingly, the values of C_s were increased for NH_4^+ adsorption onto MW and SS, and PO_4^{3-} onto TF. PO_4^{3-} adsorption onto MW seemed to be not affected by solutions ionic strength in applied concentration range (Na^+ 25–50 mM).

The increase of IS affected both the amount of adsorbed Ni^{2+}+-Co^{2+} and the reaction mechanism (Table 3S). In the presence of Na^+

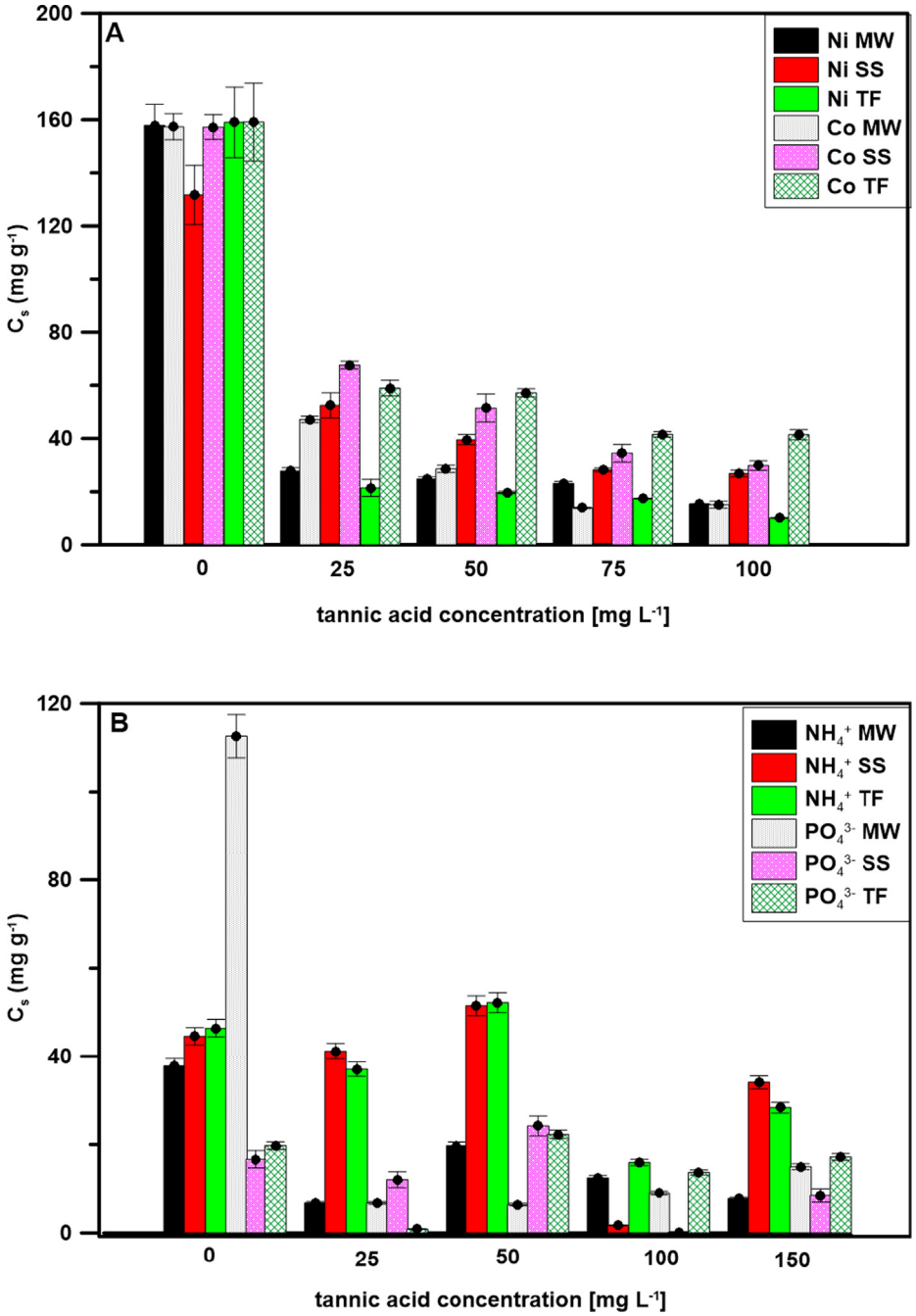

Fig. 9. DOM effect on (A) Ni^{2+}+Co^{2+} and (B) NH_4^+ + PO_4^{3-} adsorption onto TBC.

the monolayer adsorption of Ni^{2+} onto MW was noted. Ni^{2+} adsorption onto SS was changed from multilayer (*F*) to *T*. Surprisingly, Co^{2+} adsorption onto MW was directed from monolayer to multilayer formation (from *L* to *F*) indicating that more intense competition between ions and MW surface was noted [60]. Negative values of *B* (heat of adsorption) in *T* model were indicating that the adsorption process was exothermic.

DOM effect

Nickel in natural waters occurs predominantly as the ion Ni $(H_2O)_6^{2+}$ (pH 5–9) rather than in complexes with ligands, such as OH^-, SO_4^{2-}, HCO_3^-, Cl^-, and NH_3 [73]. The fate of Ni^{2+}, Co^{2+} or NH_4^+ or PO_4^{3-} in water should be affected both by pH and the presence of dissolved organic matter. Additionally, the adsorptive properties of biochar are affected by the presence of dissolved organic matter. DOM molecules are composed of hydrophobic segments with carboxylic acid and phenolic functionalities. These groups can affect the adsorption of metals or anions. Presence of mainly –COOH groups can be responsible rather for other than π–π interactions. DOM may compete with ions for adsorption sites but additionally, due to its chemical nature may form additional sites participating in adsorption onto TBC.

Generally, the addition of TA reduced the amount of Ni^{2+} and Co^{2+} adsorbed. The most sensitive to TA presence were MW during both Ni^{2+} and Co^{2+} adsorption and TF in Ni^{2+} adsorption (Fig. 9A). The effect of TA addition onto NH_4^+ + PO_4^{3-} adsorption was also noted but the data were different from Ni^{2+} and Co^{2+} adsorption. Generally, the greatest sensitivity to TA presence revealed PO_4^{3-} adsorption onto MW (Fig. 9B) and lowering of adsorption capacity with increased TA concentration was noted. The positive correlation of C_s of PO_4^{3-} adsorption onto SS ($p < 0.01$) and TF ($p < 0.05$) was noted indicating the competition of TA and PO_4^{3-} for adsorption sites onto SS and TF. The effect of DOM on NH_4^+ adsorption onto SS and TF was however different. The highest C_s was noted when TA concentration was 50 mg L^{-1} (Fig. 9B, Table S4). The data may imply that the competition between PO_4^{3-} and TA for adsorption sites on mentioned TBC was observed and TA molecules were participating in further bonding of NH_4^+.

The greatest applicability of Temkin model was noted for the adsorption of Ni^{2+} and Co^{2+} onto TBC. Monolayer mechanism was noted only when Ni^{2+} was adsorbed onto MW and the presence of TA changed the adsorption mechanism from *DR* to *L*, similarly to changed Ni^{2+} adsorption mechanism onto SS TBC (from *F* to *T*). The data clearly indicate that the presence of natural organic matter in water altered Co^{2+} and Ni^{2+} adsorption changing not only the amount being adsorbed but also the mechanism. This effect, however, was both positive and negative.

Soil application

In the literature a great attention has been paid to the application of biochar for soils [72,73]. The potential of biochar for the transformation of heavy metals [35] or organic contaminants in the contaminated soil from unstable fractions to stable fractions is established. As a result the decreased mobility and bioavailability is observed [8]. On the other hand, biochar can be also used as fertilizer for controlled release of nutrients [18]. The studies of the behavior of TBC when used in soil with concentrated NH_4^+ and PO_4^{3-} solutions is presented in Fig. 10 demonstrating some interesting observations. For NH_4^+ adsorption onto tested TBC the increase of C_S with initial concentration of NH_4^+ was noted. However, when the initial concentration was 1000 mg L^{-1}, the amount of adsorbed NH_4^+ was lower indicating that the adsorption sites onto SS or TF were limited. Generally, the behavior of MW after addition of 750 mg L^{-1} both nutrients was similar and noted *Cs* was significantly different from other concentrations. The lowest surface area offered significantly lower amount of adsorption sites. Generally, the amount of adsorbed PO_4^{3-} was lower than NH_4^+ except the highest concentration.

The obtained data clearly indicate that presented TBC has a great potential to be used as a slow-release fertilizer to improve the composition of soil elements and soil fertility [64]. Additionally, the widely observed immobilization of metals onto biochar surface may be used for metal cations fixation in contaminated soil via adsorption and complexation lowering their mobility and thus bioavailability.

Conclusions

In this study, a novel, solvent free and sustainable approach was used for development of magnetic biochar from tea waste. Co-

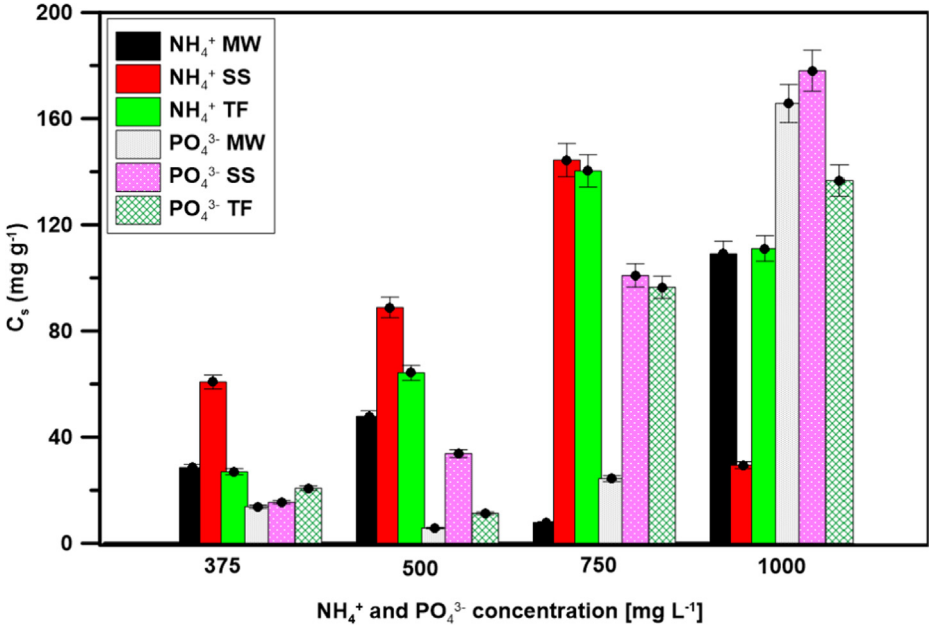

Fig. 10. Sorption of NH_4^+ and PO_4^{3-} from soil + TBC.

adsorption of NH_4^+ and PO_4^{3-} onto tested TBC was not favorable in comparison to Ni^{2+} and/or Co^{2+}. The highest amount of NH_4^+ was adsorbed onto SS and the highest amount of PO_4^{3-} was noted for MW. Highest removal capacity was observed for Co followed by Ni for all samples. The lowest removal capacity reported for PO_4^{3-} in case of SS and TF samples and then NH_4^+ for MW sample. Chemisorption was the rate limiting step during adsorption Ni and Co from single solute system and mixture solution. The process of NH_4^+ adsorption onto MW and PO_4^{3-} adsorption onto SS revealed the best fitting to Elovich model. The experimental data on Ni^{2+}, Co^{2+} and Ni^{2+}+Co^{2+}, PO_4^{3-} and NH_4^+ adsorption revealed good fitting to all tested adsorption models depending on TBC used indicating the complexity of the process and non-uniform properties of obtained TBC. The increase of the solution ionic strength affected both the amount of adsorbed Ni^{2+}+Co^{2+} and the reaction mechanism. The presence of natural organic matter in water altered Ni^{2+}+Co^{2+} and NH_4^+ + PO_4^{3-} adsorption, changing not only the amount being adsorbed but also the mechanism. This effect, however, was both positive and negative; as introduced TA molecules were participating in NH_4^+ adsorption. It is believed that the excellent results of utilization of tea waste biochar for wastewater treatment and sorption of nutrients from soil matrices can be a pathway for other food waste by considering sustainability and environmental circular economy approaches.

Data availability

The raw/processed data required to reproduce these findings cannot be shared at this time as the data also forms part of an ongoing study.

Compliance with Ethics Requirements

This article does not contain any studies with human or animal subjects.

Declaration of Competing Interest

The authors declare that they have no known competing financial interests or personal relationships that could have appeared to influence the work reported in this paper.

Appendix A. Supplementary material

Supplementary data to this article can be found online at https://doi.org/10.1016/j.jare.2021.08.001.

References

[1] Ahmad M, Rajapaksha AU, Lim JE, Zhang M, Bolan N, Mohan D, et al. Biochar as a sorbent for contaminant management in soil and water: a review. Chemosphere 2014;99:19–33. doi: https://doi.org/10.1016/j.chemosphere.2013.10.071.

[2] Beesley L, Moreno-Jiménez E, Gomez-Eyles JL, Harris E, Robinson B, Sizmur T. A review of biochars' potential role in the remediation, revegetation and restoration of contaminated soils. Environ Pollut 2011;159(12):3269–82. doi: https://doi.org/10.1016/j.envpol.2011.07.023.

[3] El-Naggar A, Shaheen SM, Hseu Z-Y, Wang S-L, Ok YS, Rinklebe J. Release dynamics of As Co, and Mo in a biochar treated soil under pre-definite redox conditions. Sci Total Environ 2019;657:686–95. doi: https://doi.org/10.1016/j.scitotenv.2018.12.026.

[4] Hailegnaw NS, Mercl F, Pračke K, Száková J, Tlustoš P. High temperature-produced biochar can be efficient in nitrate loss prevention and carbon sequestration. Geoderma 2019;338:48–55. doi: https://doi.org/10.1016/j.geoderma.2018.11.006.

[5] Lipczynska-Kochany E. Humic substances, their microbial interactions and effects on biological transformations of organic pollutants in water and soil: a review. Chemosphere 2018;202:420–37. doi: https://doi.org/10.1016/j.chemosphere.2018.03.104.

[6] Shirvanimoghaddam K, Czech B, Wiącek AE, Ćwikła-Bundyra W, Naebe M. Sustainable carbon microtube derived from cotton waste for environmental applications. Chem Eng J 2019;361:1605–16. doi: https://doi.org/10.1016/j.cej.2018.11.157.

[7] Shirvanimoghaddam K, Czech B, Wójcik G, Naebe M. The light enhanced removal of Bisphenol A from wastewater using cotton waste derived carbon microtubes. J Colloid Interface Sci 2019;539:425–32. doi: https://doi.org/10.1016/j.jcis.2018.12.090.

[8] Xiao X, Chen B, Chen Z, Zhu L, Schnoor JL. Insight into Multiple and Multilevel Structures of Biochars and Their Potential Environmental Applications: A Critical Review. Environ Sci Technol 2018;52(9):5027–47. doi: https://doi.org/10.1021/acs.est.7b0648710.1021/acs.est.7b06487.s001.

[9] Ahmed MJ, Hameed BH. Insight into the co-pyrolysis of different blended feedstocks to biochar for the adsorption of organic and inorganic pollutants: a review. J Cleaner Prod 2020;265:121762. doi: https://doi.org/10.1016/j.jclepro.2020.121762.

[10] Inyang M, Dickenson E. The potential role of biochar in the removal of organic and microbial contaminants from potable and reuse water: A review. Chemosphere 2015;134:232–40. doi: https://doi.org/10.1016/j.chemosphere.2015.03.072.

[11] Chatterjee R, Sajjadi B, Mattern DL, Chen W-Y, Zubatiuk T, Leszczynska D, et al. Ultrasound cavitation intensified amine functionalization: A feasible strategy for enhancing CO2 capture capacity of biochar. Fuel 2018;225:287–98. doi: https://doi.org/10.1016/j.fuel.2018.03.145.

[12] Bagheri A, Abu-Danso E, Iqbal J, Bhatnagar A. Modified biochar from Moringa seed powder for the removal of diclofenac from aqueous solution. Environ Sci Pollut Res 2020;27(7):7318–27. doi: https://doi.org/10.1007/s11356-019-06844-x.

[13] Wang Z, Guo H, Shen F, Yang G, Zhang Y, Zeng Y, et al. Biochar produced from oak sawdust by Lanthanum (La)-involved pyrolysis for adsorption of ammonium (NH4+), nitrate (NO3−), and phosphate (PO43−). Chemosphere 2015;119:646–53. doi: https://doi.org/10.1016/j.chemosphere.2014.07.084.

[14] Cybulak M, Sokołowska Z, Boguta P, Tomczyk A. Influence of pH and grain size on physicochemical properties of biochar and released humic substances. Fuel 2019;240:334–8. doi: https://doi.org/10.1016/j.fuel.2018.12.003.

[15] Shirvanimoghaddam K, Akbari MK, Yadav R, Al-Tamimi AK, Naebe M. Fight against COVID-19: The case of antiviral surfaces. APL Mater 2021;9(3):031112. doi: https://doi.org/10.1063/5.0043009.

[16] Czech B, Shirvanimoghaddam K, Trojanowska E, Naebe M. Sorption of pharmaceuticals and personal care products (PPCPs) onto a sustainable cotton based adsorbent. Sustainable Chem Pharm 2020;18:. doi: https://doi.org/10.1016/j.scp.2020.100324100324.

[17] Shirvanimoghaddam Kamyar, Ghasali Ehsan, Pakseresht Amirhossein, Derakhshandeh SMR, Alizadeh Masoud, Ebadzadeh Touradj, et al. Super hard carbon microtubes derived from natural cotton for development of high performance titanium composites. J Alloy Compd 2019;775:601–16. doi: https://doi.org/10.1016/j.jallcom.2018.10.121.

[18] Yi Yunqiang, Huang Zhexi, Lu Baizhou, Xian Jingyi, Tsang Eric Pokeung, Cheng Wen, et al. Magnetic biochar for environmental remediation: a review. Bioresour Technol 2020;298:122468. doi: https://doi.org/10.1016/j.biortech.2019.122468.

[19] Aravind S, Kumar PS, Kumar NS, Siddarth N. Conversion of green algal biomass into bioenergy by pyrolysis. A review. Environ Chem Lett 2020;18(3):829–49. doi: https://doi.org/10.1007/s10311-020-00990-2.

[20] Zhang Yaning, Chen Paul, Liu Shiyu, Peng Peng, Min Min, Cheng Yanling, et al. Effects of feedstock characteristics on microwave-assisted pyrolysis – a review. Bioresour Technol 2017;230:143–51. doi: https://doi.org/10.1016/j.biortech.2017.01.046.

[21] Shirvanimoghaddam Kamyar, Motamed Bahareh, Ramakrishna Seeram, Naebe Minoo. Death by waste: Fashion and textile circular economy case. Sci Total Environ 2020;718:137317. doi: https://doi.org/10.1016/j.scitotenv.2020.137317.

[22] Huang Fei, Zhang Si-Ming, Wu Ren-Ren, Zhang Lu, Wang Peng, Xiao Rong-Bo. Magnetic biochars have lower adsorption but higher separation effectiveness for Cd2+ from aqueous solution compared to nonmagnetic biochars. Environ Pollut 2021;275:116485. doi: https://doi.org/10.1016/j.envpol.2021.116485.

[23] Deng Qian, Zinoviadou Kyriaki G, Galanakis Charis M, Orlien Vibeke, Grimi Nabil, Vorobiev Eugène, et al. The effects of conventional and non-conventional processing on glucosinolates and its derived forms, isothiocyanates: extraction, degradation, and applications. Food Eng Rev 2015;7(3):357–81. doi: https://doi.org/10.1007/s12393-014-9104-9.

[24] Fakhrhoseini Seyed Mousa, Czech Bożena, Shirvanimoghaddam Kamyar, Naebe Minoo. Ultrafast microwave assisted development of magnetic carbon microtube from cotton waste for wastewater treatment. Colloids Surf, A 2020;606:125449. doi: https://doi.org/10.1016/j.colsurfa.2020.125449.

[25] Roselló-Soto Elena, Barba Francisco J, Parniakov Oleksii, Galanakis Charis M, Lebovka Nikolai, Grimi Nabil, et al. High voltage electrical discharges, pulsed electric field, and ultrasound assisted extraction of protein and phenolic compounds from olive kernel. Food Bioprocess Technol 2015;8(4):885–94. doi: https://doi.org/10.1007/s11947-014-1456-x.

[26] Ge Shengbo, Yek Peter Nai Yuh, Cheng Yoke Wang, Xia Changlei, Wan Mahari Wan Adibah, Liew Rock Keey, et al. Progress in microwave pyrolysis conversion of agricultural waste to value-added biofuels: a batch to continuous approach. Renew Sustain Energy Rev 2021;135:110148. doi: https://doi.org/10.1016/j.rser.2020.110148.

[27] Sarfarazi Messiah, Jafari Seid Mahdi, Rajabzadeh Ghadir, Galanakis Charis M. Evaluation of microwave-assisted extraction technology for separation of bioactive components of saffron (Crocus sativus L.). Ind Crops Prod 2020;145:111978. doi: https://doi.org/10.1016/j.indcrop.2019.111978.
[28] Frolova Liliya, Kharytonov Mykola. Synthesis of magnetic biochar for efficient removal of Cr(III) cations from the aqueous medium. Adv Mater Sci Eng 2019;2019:1–7. doi: https://doi.org/10.1155/2019/2187132.
[29] Akgül G, Maden TB, Diaz E, Jiménez EM. Modification of tea biochar with Mg, Fe, Mn and Al salts for efficient sorption of PO43− and Cd2+ from aqueous solutions. J Water Reuse Desal 2018;9(1):57–66. doi: https://doi.org/10.2166/wrd.2018.018.
[30] Ahmed MJK, Ahmaruzzaman M. A review on potential usage of industrial waste materials for binding heavy metal ions from aqueous solutions. J Water Process Eng 2016;10:39–47. doi: https://doi.org/10.1016/j.jwpe.2016.01.014.
[31] Ho YS, Porter JF, McKay G. Equilibrium isotherm studies for the sorption of divalent metal ions onto peat: copper, nickel and lead single component systems. Water Air Soil Pollut 2002;141(1):1–33. doi: https://doi.org/10.1023/A:1021304828010.
[32] Bourioug M, Gimbert F, Alaoui-Sehmer L, Benbrahim M, Aleya L, Alaoui-Sossé B. Sewage sludge application in a plantation: effects on trace metal transfer in soil–plant–snail continuum. Sci Total Environ 2015;502:309–14. doi: https://doi.org/10.1016/j.scitotenv.2014.09.022.
[33] "https://www.who.int/ipcs/publications/cicad/cicad69%20.pdf." [accessed].
[34] PUBLIC HEALTH STATEMENT Nickel; 2015. https://www.atsdr.cdc.gov/ToxProfiles/tp15-c1-b.pdf. [accessed].
[35] Okareh O, Enesi O. Removal of heavy metals from sewage sludge using sugarcane waste extract. J Sci Res Reports 2015;6(6):439–50.
[36] Hussain A, Priyadarshi M, Dubey S. Experimental study on accumulation of heavy metals in vegetables irrigated with treated wastewater. Appl Water Sci 2019;9(5):122. doi: https://doi.org/10.1007/s13201-019-0999-4.
[37] Xie H, Wang S, Qiu Z, Jiang J. Adsorption of NH4+-N on Chinese loess: non-equilibrium and equilibrium investigations. J Environ Manage 2017;202:46–54. doi: https://doi.org/10.1016/j.jenvman.2017.07.016.
[38] Cai R, Wang X, Ji X, Peng B, Tan C, Huang X. Phosphate reclaim from simulated and real eutrophic water by magnetic biochar derived from water hyacinth. J Environ Manage 2017;187:212–9. doi: https://doi.org/10.1016/j.jenvman.2016.11.047.
[39] Czech B, Hojamberdiev M, Bogusz A. Impact of thermal treatment of calcium silicate-rich slag on the removal of cadmium from aqueous solution. J Cleaner Prod 2018;200:369–79. doi: https://doi.org/10.1016/j.jclepro.2018.07.309.
[40] Parsimehr Hamidreza, Ehsani Ali, Goharshenas Moghadam Saba, Arachchige Dumith Madushanka Jayath Wanasinghe, Ramakrishna Seeram. Energy harvesting/storage and environmental remediation via hot drinks wastes. The Chemical Record 2021;21(5):1098–118. doi: https://doi.org/10.1002/tcr.v21.510.1002/tcr.202100018.
[41] Frank E, Varriale MC, Bristoti A. Mössbauer studies of the thermal decomposition of iron(II) ammonium sulphate hexahydrate. J Therm Anal 1979;17(1):141–50. doi: https://doi.org/10.1007/BF02156608.
[42] Heilmann I, Knudsen JM, Olsen NB, Buras B, Staun Olsen J. Studies of thermal decomposition of (NH4)2Fe(SO4)2·6H2O. Solid State Commun 1974;15(9):1481–4. doi: https://doi.org/10.1016/0038-1098(74)90921-1.
[43] Warner NA, Ingraham TR. Decomposition pressures of ferric sulphate and aluminum sulphate. Can J Chem 1960;38(11):2196–202. doi: https://doi.org/10.1139/v60-297.
[44] Zboril R, Mashlan M, Papaefthymiou V, Hadjipanayis G. Thermal decomposition of Fe2(SO4)3: demonstration of Fe2O3 polymorphism. J Radioanal Nucl Chem 2003;255(3):413–7. doi: https://doi.org/10.1023/A:1022543323651.
[45] Cao X, Prozorov R, Koltypin Y, Kataby G, Felner I, Gedanken A. Synthesis of pure amorphous Fe2O3. J Mater Res 1997;12(2):402–6. doi: https://doi.org/10.1557/JMR.1997.0058.
[46] Korolczuk M, Tyszczuk K. Application of lead film electrode for simultaneous adsorptive stripping voltammetric determination of Ni(II) and Co(II) as their nioxime complexes. Anal Chim Acta 2006;580(2):231–5. doi: https://doi.org/10.1016/j.aca.2006.07.060.
[47] "ISO, PN-EN ISO 10304-1 (2009) Water quality – determination of dissolved anions by means of ionic chromatography – part I; 2009 [accessed].
[48] "ISO, PN-EN ISO 14911 (2002) Water quality – determination of dissolved cations by means of ionic chromatography – method for waters and sewage; 2002 [accessed].
[49] Malhotra M, Suresh S, Garg A. Tea waste derived activated carbon for the adsorption of sodium diclofenac from wastewater: adsorbent characteristics, adsorption isotherms, kinetics, and thermodynamics. Environ Sci Pollut Res 2018;25(32):32210–20. doi: https://doi.org/10.1007/s11356-018-3148-y.
[50] Keerthanan S, Bhatnagar Amit, Mahatantila Kushani, Jayasinghe Chamila, Ok Yong Sik, Vithanage Meththika. Engineered tea-waste biochar for the removal of caffeine, a model compound in pharmaceuticals and personal care products (PPCPs), from aqueous media. Environ Technol Innovation 2020;19:100847. doi: https://doi.org/10.1016/j.eti.2020.100847.
[51] Shirvanimoghaddam K, Abolhasani MM, Polisetti B, Naebe M. Periodical patterning of a fully tailored nanocarbon on CNT for fabrication of thermoplastic composites. Compos A Appl Sci Manuf 2018;107:304–14. doi: https://doi.org/10.1016/j.compositesa.2018.01.015.
[52] Shirvanimoghaddam K, Czech B, Abolhasani MM, Naebe M. Sustainable periodically patterned carbon nanotube for environmental application: introducing the cheetah skin structure. J Cleaner Prod 2018;179:429–40. doi: https://doi.org/10.1016/j.jclepro.2018.01.145.
[53] Shirvanimoghaddam Kamyar, Czech Bożena, Wiącek Agnieszka E, Ćwikła-Bundyra Wiesława, Naebe Minoo. Sustainable carbon microtube derived from cotton waste for environmental applications. Chem Eng J 2019;361:1605–16. doi: https://doi.org/10.1016/j.cej.2018.11.157.
[54] Shirvanimoghaddam Kamyar, Abolhasani Mohammad Mahdi, Li Quanxiang, Khayyam Hamid, Naebe Minoo. Cheetah skin structure: A new approach for carbon-nano-patterning of carbon nanotubes. Compos A Appl Sci Manuf 2017;95:304–14.
[55] Kończak M, Oleszczuk P, Różyło K. Application of different carrying gases and ratio between sewage sludge and willow for engineered (smart) biochar production. J CO2 Util 2019;29:20–8. doi: https://doi.org/10.1016/j.jcou.2018.10.019.
[56] Lü Ting-ting, Yu De-shuang, Chen Guang-hui, Wang Xiao-xia, Huang Shuo, Liu Cheng-cheng, et al. NH4+-N adsorption behavior of nitrifying sludge immobilized in waterborne polyurethane (WPU) pellets. Biochem Eng J 2019;143:196–201. doi: https://doi.org/10.1016/j.bej.2018.12.020.
[57] Hokkanen S, Repo E, Westholm LJ, Lou S, Sainio T, Sillanpää M. Adsorption of Ni2+, Cd2+, PO43− and NO3− from aqueous solutions by nanostructured microfibrillated cellulose modified with carbonated hydroxyapatite. Chem Eng J 2014;252:64–74. doi: https://doi.org/10.1016/j.cej.2014.04.101.
[58] Wan Xia, Khan Muhammad Asim, Wang Fengyun, Xia Mingzhu, Lei Wu, Zhu Sidi, et al. Facile synthesis of protonated g-C3N4 and acid-activated montmorillonite composite with efficient adsorption capacity for PO43− and Pb(II). Chem Eng Res Des 2019;152:95–105. doi: https://doi.org/10.1016/j.cherd.2019.09.019.
[59] Santhosh Chella, Daneshvar Ehsan, Tripathi Kumud Malika, Baltrėnas Pranas, Kim TaeYoung, Baltrėnaitė Edita, et al. Synthesis and characterization of magnetic biochar adsorbents for the removal of Cr(VI) and Acid orange 7 dye from aqueous solution. Environ Sci Pollut Res 2020;27(26):32874–87. doi: https://doi.org/10.1007/s11356-020-09275-1.
[60] Li Ronghua, Wang Jim J, Zhou Baoyue, Awasthi Mukesh Kumar, Ali Amjad, Zhang Zengqiang, et al. Recovery of phosphate from aqueous solution by magnesium oxide decorated magnetic biochar and its potential as phosphate-based fertilizer substitute. Bioresour Technol 2016;215:209–14. doi: https://doi.org/10.1016/j.biortech.2016.02.125.
[61] Li Bin, Zhang Yin, Xu Jin, Xie Zhengxin, Tang Jun, Li Xuede, et al. "Simultaneous carbonization, activation, and magnetization for producing tea waste biochar and its application in tetracycline removal from the aquatic environment. J Environ Chem Eng 2021;9(4):105324. doi: https://doi.org/10.1016/j.jece:2021.105324.
[62] Khan TA, Chaudhry SA, Ali I. Equilibrium uptake, isotherm and kinetic studies of Cd(II) adsorption onto iron oxide activated red mud from aqueous solution. J Mol Liq 2015;202:165–75. doi: https://doi.org/10.1016/j.molliq.2014.12.021.
[63] Zhou S, Shao Y, Gao N, Deng J, Tan C. Equilibrium, kinetic, and thermodynamic studies on the adsorption of triclosan onto multi-walled carbon nanotubes. CLEAN – Soil, Air, Water 2013;41(6):539–47. doi: https://doi.org/10.1002/clen.201200082.
[64] Khurshid Hifsa, Mustafa Muhammad Raza Ul, Rashid Umer, Isa Mohamed Hasnain, Ho Yeek Chia, Shah Mumtaz Muhammad. Adsorptive removal of COD from produced water using tea waste biochar. Environ Technol Innovation 2021;23:101563. doi: https://doi.org/10.1016/j.eti.2021.101563.
[65] He Xianglei, Li Jialiang, Meng Qingmei, Guo Ziyu, Zhang Hao, Liu Yurong. "Enhanced adsorption capacity of sulfadiazine on tea waste biochar from aqueous solutions by the two-step sintering method without corrosive activator. J Environ Chem Eng 2021;9(1):104898. doi: https://doi.org/10.1016/j.jece:2020.104898.
[66] Li Bin, Zhang Yin, Xu Jin, Mei Yanglu, Fan Shisuo, Xu Huacheng. Effect of carbonization methods on the properties of tea waste biochars and their application in tetracycline removal from aqueous solutions. Chemosphere 2021;267:129283. doi: https://doi.org/10.1016/j.chemosphere.2020.129283.
[67] Alberti G, Amendola V, Pesavento M, Biesuz R. Beyond the synthesis of novel solid phases: review on modelling of sorption phenomena. Coord Chem Rev 2012;256(1):28–45. doi: https://doi.org/10.1016/j.ccr.2011.08.022.
[68] Hu Q, Zhang Z. Application of Dubinin-Radushkevich isotherm model at the solid/solution interface: a theoretical analysis. J Mol Liq 2019;277:646–8. doi: https://doi.org/10.1016/j.molliq.2019.01.005.
[69] Nickel in Drinking-water Background document for development of WHO Guidelines for Drinking-water Quality; 2005 [accessed].
[70] Lin D, Xing B. Tannic acid adsorption and its role for stabilizing carbon nanotube suspensions. Environ Sci Technol 2008;42(16):5917–23. doi: https://doi.org/10.1021/es800329c.
[71] de Resende MF, Brasil TF, Madari BE, Pereira Netto AD, Novotny EH. Polycyclic aromatic hydrocarbons in biochar amended soils: long-term experiments in Brazilian tropical areas. Chemosphere 2018;200:641–8. doi: https://doi.org/10.1016/j.chemosphere.2018.02.139.
[72] Gholami L, Rahimi G, Khademi Jolgeh Nezhad A. Effect of thiourea-modified biochar on adsorption and fractionation of cadmium and lead in contaminated acidic soil. Int J Phytorem 2020;22(5):468–81. doi: https://doi.org/10.1080/15226514.2019.1678108.
[73] Oleszczuk P, Kuśmierz M, Godlewska P, Kraska P, Pałys E. The concentration and changes in freely dissolved polycyclic aromatic hydrocarbons in biochar-amended soil. Environ Pollut 2016;214:748–55. doi: https://doi.org/10.1016/j.envpol.2016.04.064.